Hindawi
Shock and Vibration
Volume 2022, Article ID 8304408, 13 pages
https://doi.org/10.1155/2022/8304408

Research Article

Experimental and Numerical Study on the Earthquake Damage of Spherical Bearings for Chinese High-Speed Railway Bridge

Xin Kang,[1,2] **Mingliang Zhang**,[1,2] **Hongxi Qin**,[3] **Leqiao Zeng**,[1,2] **Linna Peng**,[1,2] **Xiaoxiang Wang**,[1,2] **Libin Deng**,[1,2] **Jia Hu**,[1,2] **Zhuo Li**,[1,2] **Guangqiang Shao**,[4] **and Qing Lin**[2]

[1]*Hunan Construction Investment Group Co LTD, Changsha 410004, China*
[2]*Hunan Construction Engineering Group Co LTD, Changsha 410004, China*
[3]*School of Civil Engineering, Central South University of Forestry and Technology, Changsha 410004, China*
[4]*South China Company, China Construction Second Engineering Bureau Co. Ltd, Shenzhen 518048, China*

Correspondence should be addressed to Hongxi Qin; hxqin@hotmail.com

Received 21 May 2022; Revised 4 October 2022; Accepted 27 October 2022; Published 10 November 2022

Academic Editor: Roberto Nascimbene

Spherical bearings are widely applied in high-speed railway bridges (HSRBs) in China. The experimental and computational analyses were carried out to help understand the damage mechanism of these bearings under earthquake loading. A shaking table test of scaled HSRB specimen (installed with spherical bearings) was performed under the simulated earthquake action, and the intensities were, respectively, 0.15 g, 0.20 g, 0.32 g, and 0.38 g (common intensities in China) of actual earthquakes in accordance with similarity relationships. After investigating and analyzing results of the shaking table test, it is shown that no damage occurred to movable bearings in all experimental earthquake scenarios, while slight damage could be found in fixed bearings at 0.32 g earthquake. Moreover, a finite element (FE) model of the prototype HSRB was established and validated. The damage degree of spherical bearings in stronger earthquakes (i.e., 0.40 g to 1.00 g) was studied through this validated FE model. The numerical results showed that the fixed bearing was completely damaged at 0.80 g earthquake, while only moderate damage occurred to the movable bearing at that intensity.

1. Introduction

Bearings could transmit the reaction force and deformation of the superstructure to the substructure [1, 2]. Therefore, the damage of bearings will mostly influence the structural safety. Currently, there are various types of bearings fabricated for bridge engineering applications. Among these bearings, the spherical bearing is increasingly used due to the following characteristics:

(1) Firstly, it can be a multidirectional movable manufacturing which meets the requirement of transmission, rotation, and movement of reaction force which is generated by the superstructure (i.e., girder).

(2) In addition, it can bear tension, compression, and transverse shear forces. Therefore, the bridges installed with the above bearings perform better than those with other bearings for earthquake-resistant design purposes.

(3) Thirdly, it is rigid enough, and the deformation under inertial force is pretty small. Thus, it ensures the smoothness and stability of the bridge when the train passes through the track.

(4) Finally, compared to other bearings, the spherical bearing is lighter, and its applicable temperature range is larger.

Therefore, due to the abovementioned redeeming features, spherical bearings are currently gaining ground in high-speed railway bridges (Figure 1), which entail high quality construction requirements.

In long-span constructions, the probability of HSRBs undergoing earthquake excitation is higher, and the

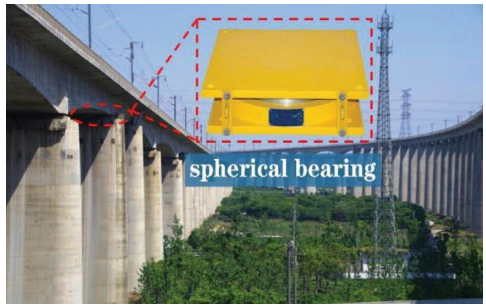

Figure 1: Spherical bearing used in a HSRB.

consequences of earthquake damage in spherical bearings are grave. Specifically, different levels of earthquake damage will directly affect whether the bearings need to be replaced, repaired, or continued to be used. Therefore, the research on seismic damage to bearings will have a great economic value [3]. Moreover, larger movements of bearings can even result in the dislodgement of the superstructure (i.e., girder) and seriously undermine the safety of the whole bridge. Thus, the earthquake damage state of spherical bearings is a matter of cardinal significance to the seismic performance of HSRBs and the safety of the moving train, which should be studied well for safety design purposes [4, 5]. Although there are a lot of numerical and experimental studies on bridge bearings, most of the research studies focus on analyzing the hysteretic energy dissipation performance of bearings and the physical characteristics of materials. There is limited research on shaking table tests that can accurately reflect earthquake excitation and the degree of damage to spherical bearings under varying earthquake intensity excitations. Therefore, the damage to spherical bearings under earthquake excitations is still unclear, and it is not possible to make a reliable assessment of possible future earthquake damage. For better understanding, relevant research studies are highly necessary to address these challenges.

Due to the limitations of test conditions, the research methods for bearings are usually carried out by quasi-static loading tests or by establishing finite element numerical models for analysis. Because these research methods cannot truly reflect the displacement response and failure characteristics of bearings under earthquake excitation, the application scope of these research methods needs to be further improved. The research method proposed in this study combines the shaking table test of the whole bridge structure and a finite element numerical analysis, which can most truly simulate the response and failure characteristics of the bearings under an earthquake. The research methodologies suggested in this work, therefore, have more obvious advantages when compared to other methods. The only disadvantage of the proposed method is that the cost of the shaking table test is higher than that of other methods.

Because of the ability to simulate seismic events, shaking table tests have been widely used in research on the seismic response of structures/components. Nowadays, there are a large amount of shaking table tests conducted to study the seismic effect of bridge bearings. For example, Takaoka et al. [6] conducted shaking table tests to study the seismic performances of slender base-isolated structures supported by laminated rubber bearings (LRBs), and the results can predict the buckling fracture of this type of bearing. Tsai et al. [7] have proven by shaking table tests that the rolling-type bearing could reduce the seismic response of structures effectively. It is shown that the seismic force transmitted by the rolling-type bearing is independent of the earthquake intensities. Li et al. [8] applied shaking table tests to study the sliding effect of the elastomeric pad bearings on the reinforced concrete bridges. The results proved the efficiency of the bearings in isolating ground motions. Yoo and Kim [9] studied the damping effects in LRBs by conducting shaking table tests, and the results illustrate that the acceleration responses of the structure decreased while the shear displacement of bearings increased. Becker and Mahin [10] validated the finite element models of triple friction pendulum bearing by shaking table tests and experiments that showed good agreement between the values and experimental results. Moreover, there was also relevant research documented about other types of bearings, for example, Oh et al. [11], Liu et al. [12], Han et al. [13], Ishida et al. [14], Yu et al. [15], Steelman et al. [16], Ponzo et al. [17], Monzon et al. [18], Abbiati et al. [19], Almazan et al. [20], Barone et al. [21], Calvi et al. [22], and Tsopelas et al. [23]. However, all of the above studies cannot be directly applied to spherical bearings which installed on the HSRB since the stiffness and seismic force of these bearings are different. Furthermore, these experiments did not study the seismic damage level of the bearings. Therefore, specific shaking table tests should be conducted to better understand the extent of damage to spherical bearings in HSRBs, especially under strong earthquakes.

To clearly understand the degree of seismic damage of spherical bearings and make a reliable assessment for future applications, a 1/12-scaled HSRB specimen (installed with scaled spherical bearings) was constructed in this research, which in accordance with specific similarity relationships. The bridge specimen was then subjected to experimental seismic excitation tests at 0.45 g, 0.60 g, 0.96 g, and 1.14 g peak ground acceleration (PGA) on the shake table. These experimental excitations, based on similarity transformations, simulated actual seismic excitations of 0.15 g, 0.20 g, 0.32 g, and 0.38 g of PGA onto the corresponding prototypes. The displacements of the spherical bearings were obtained in the shaking table test, and the seismic damage rating of each bearing was determined based on the bearing displacement limit criteria illustrated in this study. A three-dimensional numerical model of the HSRB prototype was created to better understand the level of damage to these bearings under stronger earthquakes that cannot be physically reproduced owing to the limitations in acceleration capabilities of the shake tables. This FE model was validated by the shaking table test according to similarity relationships. Therefore, the earthquake damage extent of the spherical bearing prototype under severe earthquakes (0.40 g, 0.60 g, 0.80 g, and 1.00 g for actual excitations) was investigated through this validated FE model. Overall, the experimental and numerical results can be used to evaluate the earthquake damage of existing spherical bearings installed on the HSRBs.

2. Theoretical Background for Spherical Bearing

Spherical bearings transfer loads between the superstructure (i.e., girder) and substructure (i.e., pier), while rotation is facilitated by a matching lower recessed spherical calotte. In this section, the configuration, types, and mechanical properties of such typical bearings are introduced.

2.1. Configuration of a General Spherical Bearing. There is a concave part (1) with a curved sliding sheet (2) at the bottom of spherical bearings (as shown in Figure 2). The polished hard-chromium plated surface can help the convex calotte (3) slide and improve rotations around every axis. The upper sliding sheet (4) of the calotte will move together with the sliding plate (5) above, which accommodates longitudinal and/or lateral sliding of the superstructure, if required. In order to minimize sliding resistance, the lower surface of the sliding plate is made of a polished stainless steel plate (polytetrafluoroethylene or PTFE). The motor direction of the bearings is controlled by the guide bars (6) that are allowed to move along only one axis. In order to avoid dust and debris collection, the sliding surface is often fitted with a rubber apron, which can be conveniently removed upon inspection. Alternatively, a horizontal protective cover (concertina type with a folding sheet) can be used. In the case of fixed bearings, a cover plate is placed on top of the calotte instead of a sliding plate. Moreover, anchor dowels (7), threaded sleeves, or separate anchor plates with shear studs could be installed to connect the superstructure and the substructure in this type of bearing.

2.2. Types of Spherical Bearings. Based on their ability to accommodate sliding movements, three types of spherical bearings are as follows: specifically guided sliding type (Figure 3(a)), free sliding types (Figure 3(b)), and fixed types (Figure 3(c)). The guided sliding type of spherical bearings (Figure 3(a)) means that the sliding motion along a horizontal axis could be allowed and resisting forces could be transferred in the perpendicular direction; free-sliding type (Figure 3(b)): the horizontal sliding motion could be allowed in all directions and external horizontal forces could not be transmitted; fixed type (Figure 3(c)): the bearing resists horizontal forces in every direction, allowing no sliding movements.

3. Mechanical Property of a Spherical Bearing

3.1. Lateral Load Resistance. The force distribution of the spherical bearing is shown in Figure 4, where P_D and H are the vertical and horizontal load, respectively, and β refers to the angle formed by the resultant force. The resulting load is presumed to be transmitted in a circular concave region (depicted with the bold line in Figure 4).

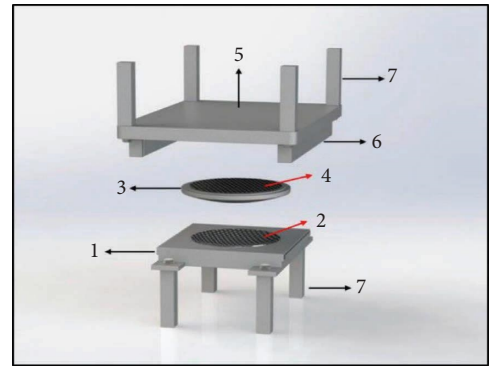

Figure 2: Configuration of a spherical bearing.

Each equal length (radii of the contact area) corresponds to an angle (ψ-β). When the concave plate of the bearing undergoes rotation by angle θ, the projection of the circular concave area is a circular area with a radius equal to R sin (ψ-β-θ). Similarly, the resultant force is $H/\sin\beta$. Therefore, the average contact stress on the PTFE is as follows:

$$\sigma_{PTFE} = \frac{\text{Force}}{\text{Area}} = \frac{H/\sin\beta}{\pi\left(R\sin\left(\psi - \beta - \theta\right)^2\right.}. \quad (1)$$

Therefore, the maximum lateral load resistance can be calculated using the following equation:

$$H \le \pi R^2 \sigma_{PTFE} \sin^2\left(\psi - \beta - \theta\right)\sin\beta. \quad (2)$$

3.2. Rotation Resistance. A spherical bearing resists rotation through the development of the moment (as shown in (3)). This moment, in relation to the pivot point located at distance R from the spherical surface, is easily shown to be given by the following equation in which P is the vertical load and μ is the coefficient of friction at the spherical surface (as shown in Figure 5):

$$M = \mu \text{PR}. \quad (3)$$

This moment of the bearing is equal to $2\mu PR$ in the case of a flat sliding surface and equal to μPR when only the spherical part exists.

4. Shaking Table Test

4.1. Experimental Specimen. Shaking table tests were performed to study the earthquake damage of spherical bearings which applied in Chinese HSRBs. Nevertheless, because of the acceleration capacity limitations and the shake table restriction, the bridge prototype (all components, including the spherical bearings) was scaled according to the similarities (Table 1) and the final simulation parameters are shown in Table 2 [24]. The physical parameters of the bearing specimen are shown in Table 3; the layout of the scaled girder and piers are shown in Figures 6 and 7. The design of the bridge and bearing specimens was based on relevant Chinese seismic specification [25, 26]. The results of

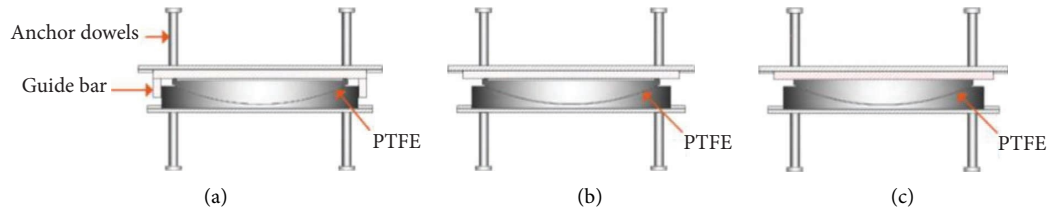

Figure 3: Different types of spherical bearings: (a) guided sliding bearing, (b) free sliding bearing, and (c) fixed bearing.

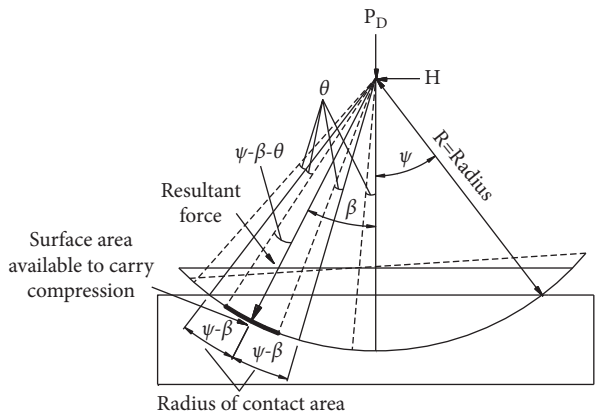

Figure 4: Force distribution of a spherical bearing.

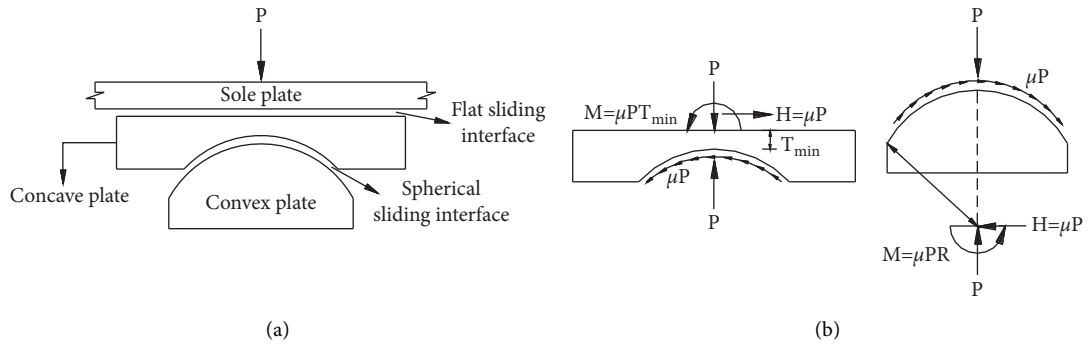

Figure 5: Diagram of a spherical bearing under vertical load and rotation.

Table 1: Physical dimension of parameters.

Physical	System	Physical	System
Length	L	Stiffness	MT^{-2}
Displacement	L	Density	MT^{-3}
Time	T	Force	MLT^{-2}
Mass	M	Moment	ML^2T^{-2}
Stress	$ML^{-1}T^{-2}$	Velocity	L^2T^{-1}
Strain	1	Acceleration	LT^{-2}
Modulus	$ML^{-1}T^{-2}$	Damp	ML^{-1}

the cyclic loading tests on spherical bearings can be obtained from the bearing manufacturers [27].

4.2. Test Setup and Instrumentation. Following the similarity relations, the bridge specimen used concrete and lead blocks as added weight to guarantee the required density in terms of the similarity relationships (Sp = 4, see Table 2), which is characterized by uniformity along the tracks and piers. The final assembled experimental specimen is shown in Figure 8. In addition, this specimen was also instrumented with different data acquisition devices, as shown in Figure 9, to obtain displacement time history.

4.3. Loading Scheme. The HSR bridges constructed in China are generally subjected to earthquakes with characteristic periods of 0.1 s to 0.4 s and common strengths not exceeding 0.38 g [28]. The El-Centro wave was selected, and after similarity transformation (S_a = 3, Table 2), the PGA scales of experimental earthquake intensity were adjusted to 0.45 g, 0.60 g, 0.96 g and 1.14 g, respectively. They corresponded to actual earthquake excitation of 0.15 g, 0.20 g, 0.32 g, and 0.38 g PGA. As an example of excitation, a 0.45 g PGA

Table 2: Similitude parameters and similarity ratios of the shaking table test [24].

Property	Physical quantity	Similarity relation	Ratio
Material	Modulus*	S_E	1
	Stress	$S_\sigma = S_E$	1
	Density	$S_\rho = S_\sigma / S_a S_l$	4
Load	Point load	$S_P = S_E S^2{}_l$	1/144
	Line load	$S_\omega = S_E S_l$	1/12
	Area load	$S_q = S_E$	1
Geometric	Length*	S_l	1/12
	Displacement	$S_d = S_l$	1/12
	Area	$S_A = S^2{}_l$	1/144
Dynamic	Acceleration*	S_a	3
	Mass	$S_m = S_\rho S^3{}_l$	4/1728
	Period	$S_T = S_l\ (S_\rho S^{-1}{}_E)^{0.5}$	1/6

(* indicates a base parameter).

Table 3: Physical parameters of spherical bearing specimen.

Vertical bearing capacity (kN)	1000
Bearing corner (rad)	0.02
Horizontal bearing capacity (kN)	5%~10% of vertical capacity
Design displacement (mm)	±100, ±40 ± 3, 0 (almost)
Design friction coefficient	$\mu \leq 0.03$
Applicable temperature range	−40°C ~ +60°C
Elastic modulus of bearing (MPa)	210000
Density of bearing (kg/m^3)	7850
Poisson's ratio of bearing	0.2
Elastic modulus of PTFE (MPa)	1500
Density of PTFE (kg/m^3)	2200
Poisson's ratio of PTFE	0.4

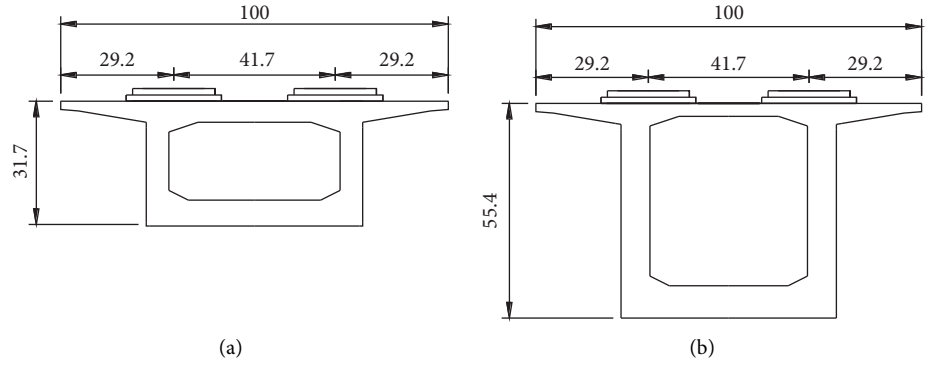

Figure 6: Specimen of girder section for (a) minimum section and (b) maximum section (unit: cm).

earthquake was used in the shaking table test with an acceleration spectrum, as shown in Figure 10.

In addition, to understand the difference in earthquake damage of scaled bearings between the specimens subjected to unidirectional and bi-directional excitations, the experimental earthquakes were classified into two types. Specifically, (1) unidirectional earthquake excitation was excited in the x (represented as x_p) or y (represented as y_p) direction, and (2) bi-directional earthquake excitation was excited in both x- and y directions simultaneously and represented as $(x_p + y_s)$ or $(x_s + y_p)$. For the bi-directional earthquakes, the primary effects of an earthquake in the x or y directions were defined as x_p or y_p, respectively. Moreover, to consider the torsional coupling interaction, the intensity of the secondary earthquake (e.g., x_s or y_s) was 0.85 times smaller than the primary PGA according to the Chinese specification GB50011-2010. Table 4 gives the experimental sequence.

5. Experimental Results

The arrangement of scaled spherical bearings (including movable and fixed bearings) for this HSRB specimen (continuous girder bridge) is shown in Figure 11. Specifically, the lateral-movable (5#) and fixed bearing (6#) were installed on the top of Pier 3, while multiway-movable (1#, 3#, and 7#) and longitudinal-movable bearings (2#, 4#, and

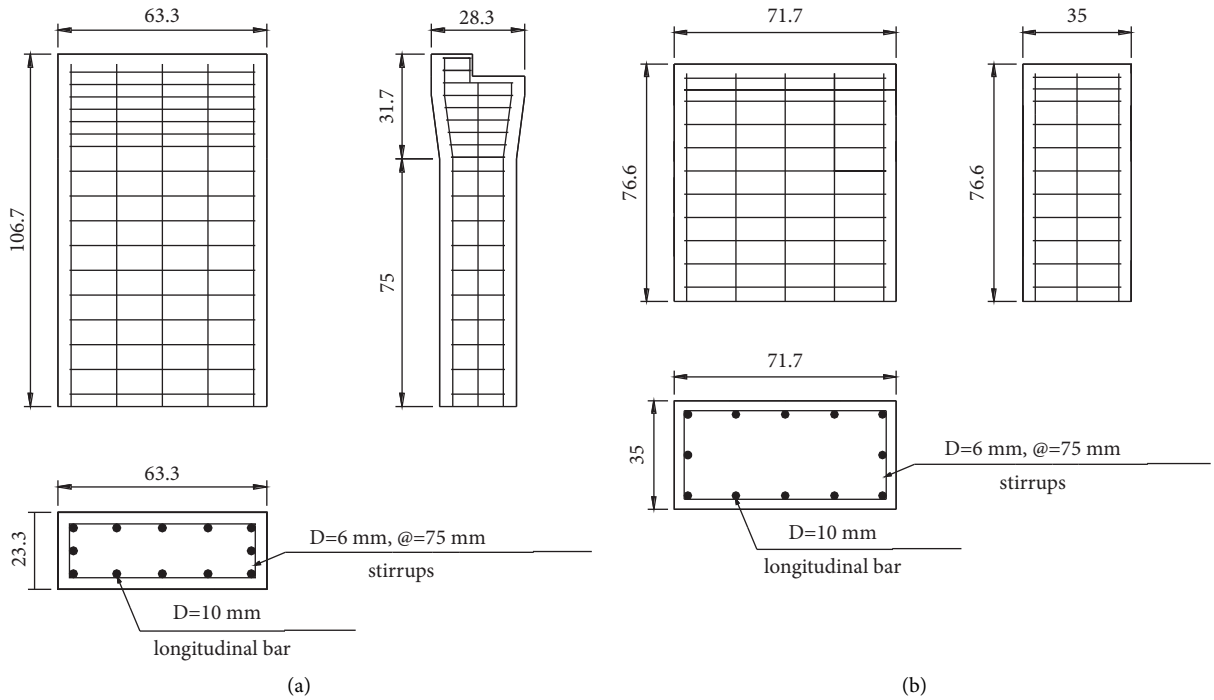

Figure 7: Specimen of pier drawings for (a) side piers (Pier-1 and Pier-4) and (b) main piers (Pier-2 and Pier-3) (unit: cm).

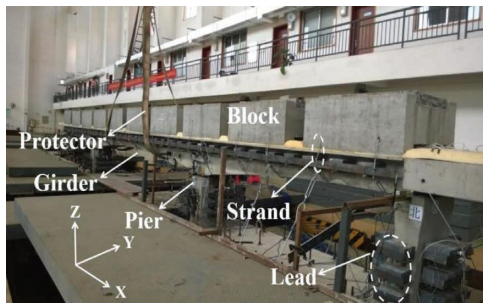

Figure 8: HSRB test specimen.

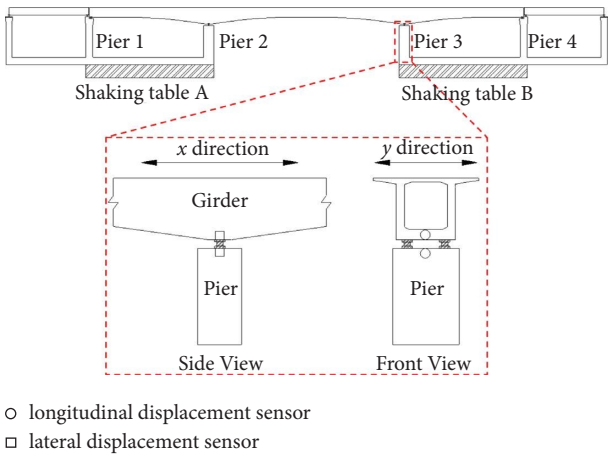

Figure 9: Arrangement of sensors in the x and y direction.

8#) were installed on the tops of Pier 1, Pier 2, and Pier 4, respectively. In this section, the displacement of scaled spherical bearings under earthquakes was studied based on the shaking table test results. The experimental results can be used directly to better evaluate the displacement and possible damage of existing spherical bearings applied in prototype HSRBs (linked to the similarity relationships, see Table 2).

5.1. Earthquake Displacement. The earthquake displacement of each scaled bearing (arranged as Figure 11(a)) during the tests was observed by obtaining the relative displacement between each pier and continuous girder. For example, Figure 12 illustrates the relative displacement between Pier 1 and the continuous girder under test scenarios, which reflect the displacement of bearing 1 and bearing 2 according to the instrumentation arrangement (Figures 9 and 11(a)). It is reasonable to find that the displacement of these two bearings (bearing 1 and bearing 2) increased with increasing experimental earthquake intensity (i.e., from 0.45 g to 1.14 g). The seismic force ($F = MA$) has a correspondingly enhanced effect on the bearing. Moreover, compared to the displacement in the y direction (Figure 10(b)), a significant residual displacement can be seen in the x direction (Figure 10(a)) after earthquake excitation. This result can be attributed to the fact that bearing 1 and bearing 2 are longitudinally movable. Therefore, an irrecoverable displacement occurred after earthquake excitation in the x direction. In addition, these residual displacements become more obvious with the increase of earthquake intensity (e.g., at 1.14 g, see in Figure 12(a)). Therefore, the experimental results illustrate that, for the prototype HSRB, the girder has an obvious residual displacement after 0.38 g earthquake excitation in the x direction (corresponding to the similarity relationships (Table 2)), which will affect the safety of the

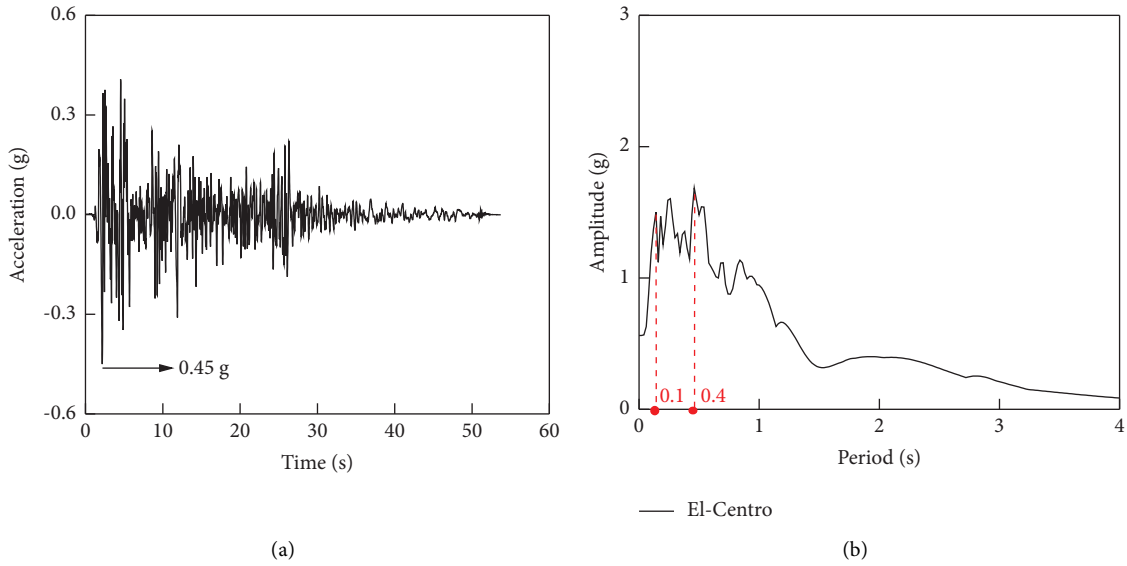

Figure 10: El-cento earthquake wave showing (a) acceleration time history and (b) the acceleration spectrum.

Table 4: Test scenarios in sequence.

Test scenario	Input earthquake	Earthquake direction	Experimental PGA scale (g)	
1	White noise excitation		0.05	0.05
2	0.15 g (PGA) earthquake	El-Centro (x_p)	0.45	N.A.
3		El-Centro (y_p)	N.A.	0.45
4		El-Centro ($x_p + y_s$)	0.45	0.38
5		El-Centro ($x_s + y_p$)	0.38	0.45
6	White noise excitation		0.05	0.05
7	0.20 g (PGA) earthquake	El-Centro (x_p)	0.60	N.A.
8		El-Centro (y_p)	N.A.	0.60
9		El-Centro ($x_p + y_s$)	0.60	0.51
10		El-Centro ($x_s + y_p$)	0.51	0.60
11	White noise excitation		0.05	0.05
12	0.32 g (PGA) earthquake	El-Centro (x_p)	0.96	N.A.
13		El-Centro (y_p)	N.A.	0.96
14		El-Centro ($x_p + y_s$)	0.96	0.82
15		El-Centro ($x_s + y_p$)	0.82	0.96
16	White noise excitation		0.05	0.05
17	0.38 g (PGA) earthquake	El-Centro (x_p)	1.14	N.A.
18		El-Centro (y_p)	N.A.	1.14
19		El-Centro ($x_p + y_s$)	1.14	0.97
20		El-Centro ($x_s + y_p$)	0.97	1.14
21	White noise excitation		0.05	0.05

bridge structure (e.g., collision with an adjacent span) and stability of a high-speed moving train.

Furthermore, the maximum displacement of the bearing obtained from all test scenarios is given in Table 5 (x direction) and Table 6 (y direction). Results show that the bearings installed on the side piers (Pier-1 and Pier-4) have a larger maximum x-direction displacement and y-direction displacement than the main piers (Pier-2 and Pier-3). This is because the stiffness (EI_x and EI_y) of side pies is lower than that of the main piers. Therefore, the displacement at the top of side piers is larger under earthquake excitation, which results in a larger relative displacement between the pier and girder (bearing displacement). Moreover, due to the difference in pier stiffness in x and y direction (i.e., $EI_x < EI_y$), the displacement of each pier in the x direction is larger than in the y direction when subjected to the same intensity of earthquake excitation. Thus, the displacement of bearings in the x direction is correspondingly more obvious than that in the y direction. In addition, the experimental results also show that bi-directional earthquake excitation ($x_p + y_s$ or $y_p + x_s$) affects the safety of bearings more since the maximum displacement of bearings under those earthquakes is larger than that of under single-directional earthquake excitation (x_p or y_p). This result could offer reasonable

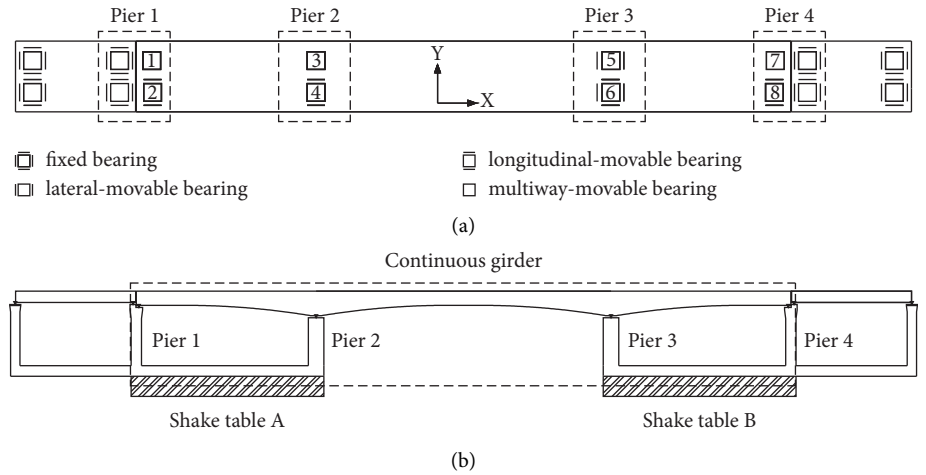

FIGURE 11: Spherical bearings' arrangement in the experimental HSRB (continuous girder) specimen for (a) plane view and (b) vertical view.

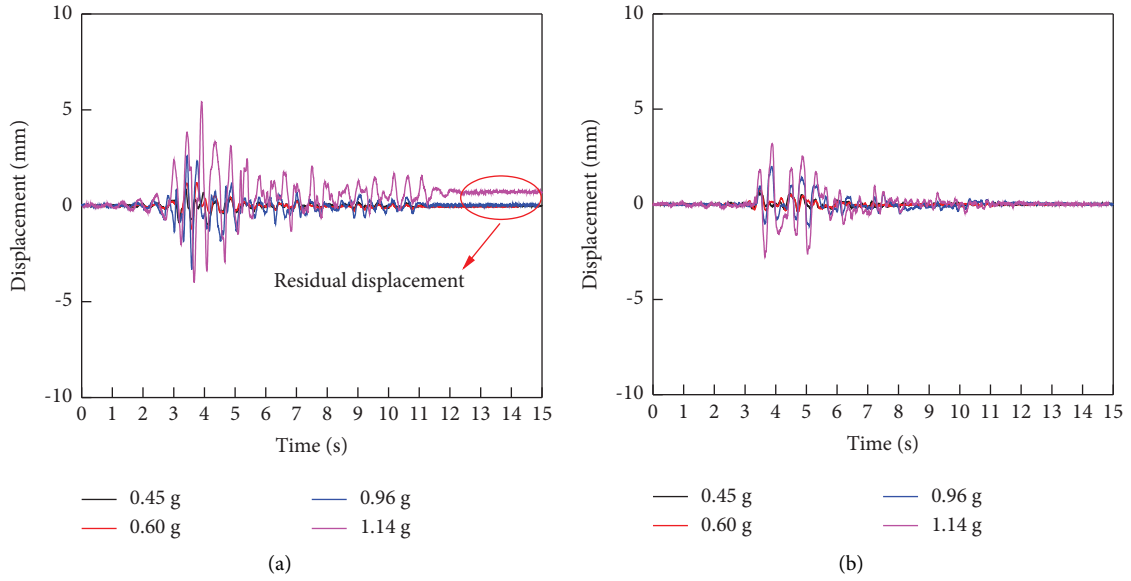

FIGURE 12: Relative displacement of Pier 1 and the continuous girder under different earthquake intensities for (a) x direction and (b) y direction.

explanations given the fact that the piers are more vulnerable under bi-directional excitation due to the coupling dynamic effects of x-and y-direction earthquakes.

5.2. Earthquake Damage. The movement of a bearing may exceed the maximum displacement limits when subjected to earthquakes, which results in different levels of damage to these bearings. Therefore, the earthquake damage of spherical bearings should be studied well for a better safety assessment. However, it is difficult to define the categories or levels of earthquake damage to spherical bearings, since there are few relevant research studies accumulated, especially for the spherical bearings applied in the HSRBs. In this section, the maximum displacement limits for a prototype spherical bearing according to relevant research are given in Table 7. Moreover, the levels of damage thresholds are estimated [29, 30], and the degree of damage and the corresponding classification are shown in Table 8. Finally, the damage evaluation of prototype spherical bearings under different earthquakes is studied.

Based on the experimental results obtained and combined with the similarity relationships (Table 2), the prototype multidirectionally movable, longitudinally movable, and transversely movable spherical bearings (in the arrangement shown in Figure 9(a)) were not damaged when subjected to actual PGA earthquakes of 0.15 g to 0.38 g. This could be explained by the fact that the seismic forces in the superstructure are mainly carried by the fixed bearings. Therefore, the relative displacement of piers (i.e., Pier 1, Pier 2, and Pier 4) and girders were below the maximum displacement limits (Table 6), and no damage occurred in these bearings during the earthquakes. However, damage could also be found in the fixed bearings, the extent of which (in

Table 5: Maximum relative displacement (unit: mm) between each pier and continuous girder under different experimental earthquake intensities (in x direction).

Intensity (g)	Pier 1		Pier 2		Pier 3		Pier 4	
	x_p	$x_p + y_s$	x_p	$x_p + y_s$	x_p	$x_p + y_s$	x_p	$x_p + y_s$
0.45	1.0	1.3	2.9	3.3	0.1	0.2	1.7	2.3
0.60	1.2	1.6	3.4	3.9	0.1	0.2	2.2	2.9
0.96	3.3	4.0	4.3	5.1	0.2	0.3	3.5	4.0
1.14	5.4	6.1	6.0	6.9	0.2	0.3	5.2	5.9

Table 6: Maximum relative displacement (unit: mm) between each pier and continuous girder under different experimental earthquake intensities (in y direction).

Intensity (g)	Pier 1		Pier 2		Pier 3		Pier 4	
	y_p	$y_p + x_s$	y_p	$y_p + x_s$	y_p	$y_p + x_s$	y_p	$y_p + x_s$
0.45	0.6	0.8	1.7	2.0	0.1	0.1	1.0	1.4
0.60	0.7	1.0	2.0	2.3	0.1	0.1	1.3	1.7
0.96	2.0	2.4	2.6	3.1	0.1	0.2	2.1	2.4
1.14	3.2	3.7	3.6	4.1	0.1	0.2	3.1	3.5

Table 7: Maximum displacement limits of spherical bearings.

Bearing type	Maximum displacement limits (unit: mm)	
	Longitudinal direction	Lateral direction
Multimovable bearing	100	40
Longitudinal-movable bearing	100	3
Lateral-movable bearing	3	100
Fixed bearing	0 (almost)	0 (almost)

Table 8: Damage threshold of spherical bearings.

Bearing type	Damage threshold (maximum displacement, unit: mm)			
	Slight	Moderate	Severe	Complete
Bearing (fixed)	2	4	6	8
Bearing (movable)	100	130	160	200

relation to Table 8) is shown in Figure 13. To be specific, the fixed bearing was not damaged when subjected to PGAs of 0.15 g to 0.20 g x-direction earthquakes (x_p), while slight damage could be seen as the intensity increased to 0.32 g and 0.38 g (Figure 13(a)). Moreover, due to dynamic coupling, the fixed bearing is susceptible under bi-directional excitation ($x_p + y_s$), as slight damage can be found in all earthquake scenarios (i.e., from 0.15 g to 0.38 g) when under bi-directional excitation. However, because of the different stiffness ($EI_x < EI_y$), the relative displacement between the pier and the beam in the y direction is smaller than the relative displacement in the x direction (Figure 13(b)). Therefore, the level of seismic damage to the fixed bearing in the y direction is correspondingly smaller than that in the x direction. Specifically, no damage to the fixed spherical bearing was observed for the y-direction earthquake (y_p) from 0.15 g to 0.38 g PGA, and slight damage could be seen in the ($y_p + x_s$) earthquakes when the intensity exceeded 0.32 g.

6. Numerical Analysis

Due to the accelerating ability limitations of shake tables, more severe earthquakes (e.g., beyond 1.14 g PGA) cannot be produced by the shaking tables to excite the HSRB specimen. Therefore, the earthquake intensity of severe or complete damage to bearings (linked to Table 8) is still not well understood, which makes it important for researchers to consider whether to replace or just maintain those damaged bearings. To address the above problem, a FE model of a prototype HSRB was modelled (by *OpenSEES*) and validated with the experimental results from the shake table testing in accordance with the similarity relationships.

6.1. Finite Elements' (FE) Modeling. In this FE model, the piers were established by nonlinear beam-column elements with fiber sections. The connection components, such as the slide layer, CA mortar, and the bearing, were modelled using perfectly elastic plastic material. Moreover, linear beam-column elements were applied to model the girder (simply supported and continuous girder), ballastless track system, and rails. The material and section properties of these elements, such as elastic modulus, section area, and rotational inertia and torsion constants, were determined by the prototype HSRB. In addition, Giuffre–Menegotto–Pinto steel material (Steel 02) and Kent–Scott–Park concrete material (Concrete 02) were used to model the constitutive relationships of rebar and concrete, respectively, with the parameters obtained from the material test. To simulate the hysteresis behaviors of each component under earthquake excitation, an ideal elastoplastic hysteresis model was applied in HSRB modeling [31].

6.2. FE Validation. The FE model is validated in this section using similarity transformations. Specifically, to compare with the results of shaking table tests, the time domain and displacement of numerical calculation results are scaled at 1/6 and 1/12 scaled according to the similarity relationships (Table 2). For example, the displacement comparison between the test and experimental results (connected with similarity transformations) for a fixed spherical bearing (6#) under earthquake excitation in the x direction (0.45 g) is shown in Figure 14. It can be seen that the comparison of time histories was reasonably consistent. This is due to the consideration of integrating the establishment of the FE model with the effect of the three-span simply supported girders located in the beam end of the continuous girder bridge, while only one span of the adjacent simply supported girder bridge was constructed in the experiment in view of the dimensional limitation of shake tables.

In addition, the displacement of bearings installed on the same pier is consistent (e.g., 1# and 2# on the Pier 1). Therefore, experimental and numerical results (under 0.45 g PGA) of the maximum displacements of some typical bearings (2#, 4#, 6#, and 8#) were compared to validate the FE model (Table 9). The

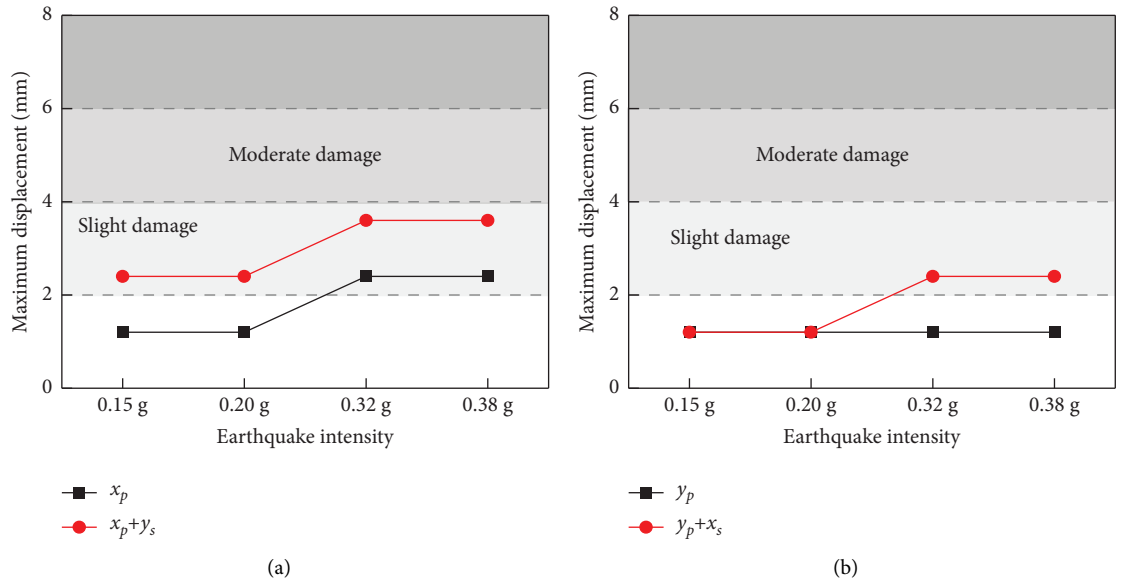

Figure 13: The maximum displacement and damage level of a fixed spherical bearing (6 #) under different earthquake intensities, for (a) x direction and (b) y direction.

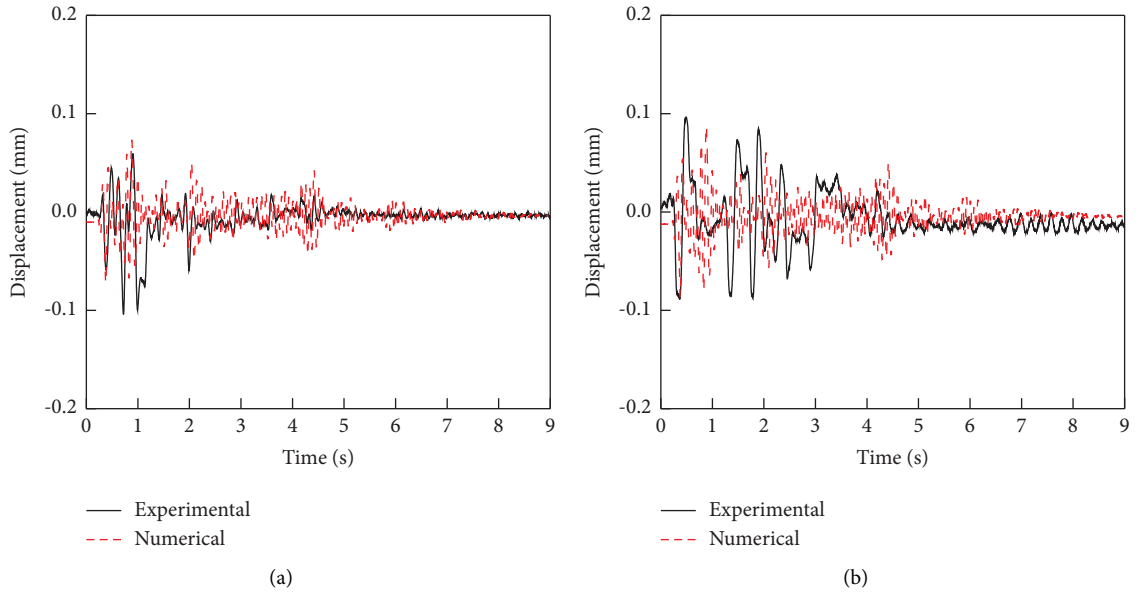

Figure 14: Comparison between testing and calculation results of fixed bearing (6#) for (a) x direction and (b) y direction.

Table 9: Comparison of maximum displacement of typical bearings (under 0.45 g) for the experimental test and FE model (mm).

Earthquake direction	Bearing number	Test (mm)	FE model (mm)	Difference (%)
x direction (x_p)	2 #	1.03	0.83	19.42
	4 #	2.89	2.10	27.34
	6 #	0.12	0.08	33.33
	8 #	1.71	1.36	20.47
y direction (y_p)	2 #	0.63	0.56	11.11
	4 #	1.68	1.45	13.69
	6 #	0.09	0.06	33.33
	8 #	1.34	1.15	14.18

Note. difference = (test result–FE model result)/test result × 100%.

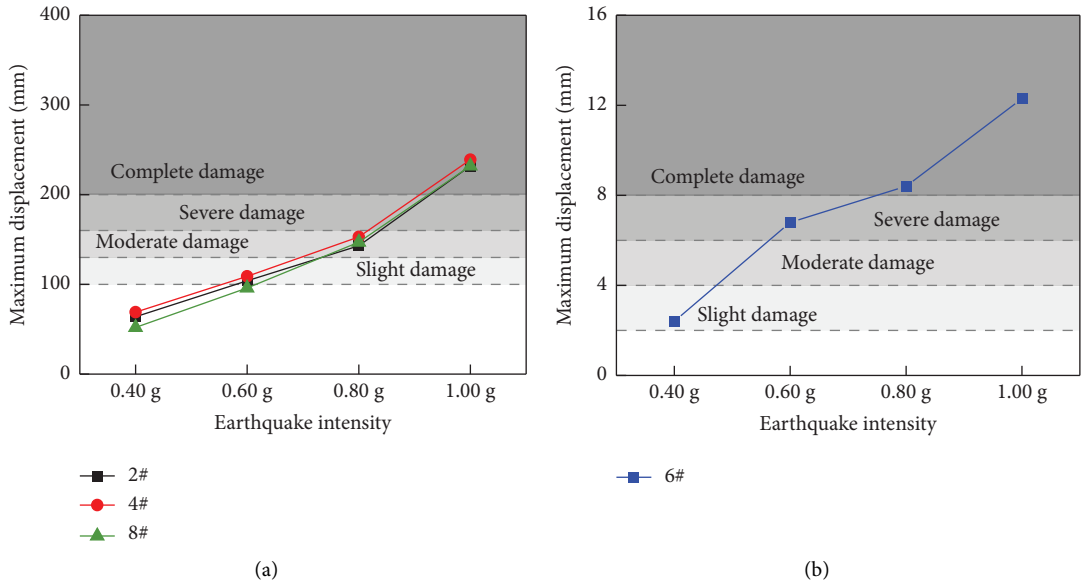

Figure 15: Damage levels of bearings under different earthquake intensities, for (a) longitudinal-movable bearings (2#, 4#, and 8#) and (b) fixed bearing (6#).

comparison results show that the maximum difference (around 33.33%) can be seen in the fixed bearing (6#), while relatively less difference can be found in the bearing 2# (about 19.42% and 11.11% for x and y direction, respectively). This may be due to the fact that fixed bearings are more vulnerable in earthquakes since the seismic forces on the superstructure are mainly carried by this bearing. Therefore, its (fixed bearing, 6#) displacement is more easily affected by the experimental environment than that of other movable bearings (2#, 4#, and 8#). However, the differences obtained seem to be acceptable, and therefore, this modeling approach can be used for more detailed damage evaluation and parametric studies in the following investigation.

6.3. Parametric Analysis. The experimental results show that the bearings were more vulnerable in the x direction (detailed in the previous section). Therefore, to predict the damage level of spherical bearings subjected to more severe x-direction earthquakes, parametric analysis is performed by use of a validated FE model. Specifically, the excited earthquakes are enlarged to 4 different intensities (i.e., 0.40 g, 0.60 g, 0.80 g, and 1.00 g) and the maximum displacement and damage level of spherical bearings are studied in this section. For example, the damage levels of typical bearings (2#, 4#, 6#, and 8#) under these earthquakes are illustrated in Figure 15.

Calculation results show that the fixed spherical bearing (6#) is more vulnerable since it was slightly damaged when subjected to the PGA scale of 0.40 g seismic excitation (Figure 15(b)), while other longitudinal-movable bearings (2#, 4#, and 8#) suffered no damage at that intensity (Figure 15(a)). Moreover, the superstructure mass of #4 support is relatively larger than that of 2# and 8#, and its seismic force ($F = MA$) is correspondingly higher. Therefore, this resulted in a marginally larger damage level in 4# than that of 2# and 8# (Figure 15(a)). In addition, it is reasonable to find that the damage level of all analyzed bearings increased with the increasing earthquake intensity, since the seismic force on the bearings was enhanced accordingly. In the end, completed damage can be found in the fixed bearing (6#) when subjected to the 0.80 g earthquake. Therefore, it should be replaced or changed for safety consideration. However, longitudinal-movable bearings (2#, 4#, and 8#) are only moderately damaged at that intensity (0.80 g), which means that they can still be used. Interestingly, all bearings are completely damaged when subjected to the PGA scale of 1.00 g earthquake. Thus, the girder will fall off at that intensity (1.00 g).

7. Conclusions

A scaled HSRB specimen installed with spherical bearings was fabricated and tested using shaking table apparatus to evaluate the seismic damage level of spherical bearings under seismic excitation of 0.15 g, 0.20 g, 0.32 g, and 0.38 g PGA, which are often experienced in China. Considering the acceleration limitations in shake tables, a FE model of a prototype HSRB was established and validated to study the earthquake damage of these bearings under more severe earthquakes (i.e., 0.40 g, 0.60 g, 0.80 g, and 1.00 g). Specifically, the following conclusions can be obtained from this study:

(1) As the effects of other bridge components (e.g., girder and pier) on the seismic behavior of spherical bearings were considered in the test, the earthquake results were more consistent with the actual bridges. Therefore, the experimental method is more reliable than those who just study the bearings.

(2) Experimental results show that the movable bearings (longitudinal-movable, lateral-movable, and multi-way-movable bearings) almost suffered no damage under experimental earthquake scenarios (0.15 g to

0.38 g linked to the similarity relationship) in both x (longitudinal) and y (lateral) direction. However, the fixed bearing is slightly damaged at 0.32 g in x direction, while no damage could be found in y direction. Moreover, experimental results also show that the bearings in x direction are more vulnerable than those in y direction, which means earthquake protection of the HSRB should pay more attention to longitudinal earthquake excitation. In addition, due to the effects of coupling vibration, the bearings are more easily damaged under bi-directional earthquake excitation (i.e., $x_p + y_s$ or $y_p + x_s$) than under unidirectional earthquake (i.e., x_p or y_p).

(3) A FE model was established to study the earthquake damage level of bearings under more severe seismic excitations. Since the results of the shaking table tests supported the accuracy of this FE model, the modeling strategy may be used or developed for additional in-depth research.

(4) Earthquake damage level of spherical bearings (x direction) under severe earthquakes (0.40 g to 1.00 g) is studied by using this validated FE model. Calculation results show that the fixed bearing will completely damage at an early 0.80 g, and therefore , it should be replaced or changed, while only moderate damage can be seen in those movable bearings at that intensity.

The research in this study can help researchers understand in detail the damage level of spherical bearings under different earthquake intensities. Moreover, it also helps researchers determine whether to repair, replace, or continue to use the bearings after the earthquake. Therefore, the research results of this study will have great engineering application value and economic benefits for the high-speed railway bridge construction.

Theoretical study of existing energy-damping bearings and choosing the appropriate bearing restoring force model should be used to deduce the theoretical equations, which are needed to calculate bearing mechanical parameters subsequently. In addition, a reasonable finite element model should also be established to study the energy consumption and hysteretic performance of spherical bearings.

Data Availability

Some or all of the data, models, or code supporting the results of this study can be obtained from the corresponding author upon reasonable request.

Conflicts of Interest

The authors declare that there are no conflicts of interest regarding the publication of this paper.

Acknowledgments

This research was supported by the Hunan Construction Investment Group Co., Ltd, the Natural Science Foundation of Hunan Province (Grant nos. 2020JJ4947 and 2018JJ3672), and the Central South University.

References

[1] A. A. Adamov, A. A. Kamenskikh, and A. P. Pankova, "Influence analysis of the antifriction layer materials and thickness on the contact interaction of spherical bearings elements," *Lubricants*, vol. 10, no. 2, p. 30, 2022.

[2] Y. Yang, Y. Zhang, and J. Ju, "Study on the mechanical properties of a type of spherical bearing," *Journal of Theoretical and Applied Mechanics*, vol. 59, no. 4, pp. 539–550, 2021.

[3] X. Hong, W. Guo, and Z. Wang, "Seismic analysis of coupled high-speed train-bridge with the isolation of friction pendulum bearing," *Advances in Civil Engineering*, vol. 2020, pp. 1–15, Article ID 8714174, 2020.

[4] L. Jiang, S. Cao, and B. Wei, "Effects of friction-based fixed bearings on seismic performance of high-speed railway simply supported girder bridges and experimental validation," *Advances in Structural Engineering*, vol. 22, no. 3, pp. 687–701, 2019.

[5] Y. B. Ma, B. Zhao, and B. D. Gu, "Random vibration analysis of spherical anti-seismic bearing," *Applied Mechanics and Materials*, vol. 638, no. 640, pp. 1834–1837, 2014.

[6] E. Takaoka, Y. Takenaka, and A. Nimura, "Shaking table test and analysis method on ultimate behavior of slender base-isolated structure supported by laminated rubber bearings," *Earthquake Engineering & Structural Dynamics*, vol. 40, no. 5, pp. 551–570, 2011.

[7] M. H. Tsai, S. Y. Wu, K. C. Chang, and G. C. Lee, "Shaking table tests of a scaled bridge model with rolling-type seismic isolation bearings," *Engineering Structures*, vol. 29, no. 5, pp. 694–702, 2007.

[8] J. Z. Li, H. Tang, and Z. G. Guan, "Shake table test and numerical analysis of a bridge model supported on elastomeric pad bearings," *Journal of Earthquake Engineering*, vol. 21, no. 4, pp. 604–634, 2017.

[9] B. Yoo and Y. H. Kim, "Study on effects of damping in laminated rubber bearings on seismic responses for a ? scale isolated test structure," *Earthquake Engineering & Structural Dynamics*, vol. 31, no. 10, pp. 1777–1792, 2002.

[10] T. C. Becker and S. A. Mahin, "Experimental and analytical study of the bi-directional behavior of the triple friction pendulum isolator," *Earthquake Engineering & Structural Dynamics*, vol. 41, no. 3, pp. 355–373, 2012.

[11] J. Oh, C. Jang, and J. H. Kim, "Seismic behavior characteristic of high damping rubber bearing through shaking table test," *Journal of Vibroengineering*, vol. 18, no. 3, pp. 1591–1601, 2016.

[12] H. Liu, X. Wang, and J. Liu, "The shaking table test of an SMA strands-composite bearing," *Journal of Earthquake Engineering and Engineering Vibration*, vol. 022, no. 3, pp. 134–157, 2008.

[13] Q. Han, X. L. Du, J. B. Liu, and W. G. Liu, "Seismic response of isolated bridges with lrb under muldi-directional earthquake——part (I) shaking table test of bridge model," *Journal of Vibration and Shock*, vol. 27, no. 9, pp. 59–183, 2008.

[14] K. Ishida, H. Shiojiri, G. Yoneda, and A. Matsuda, "Shaking table test on ultimate behavior of seismic isolation system. Part 2: response behavior of rubber bearings," *Proceedings of the World Conference on Earthquake Engineering*, , Barcelona, Spain, January 1992.

[15] X. Yu, J. Zai, and Z. Wang, "Shaking table model test on lead core rubber bearing in isolation structure system considering SSI," *Journal of Nanjing University of Aeronautics & Astronautics*, vol. 6, no. 42, pp. 786–792, 2010.
[16] J. Steelman, E. Filipov, L. Fahnestock et al., "Experimental behavior of steel fixed bearings and implications for seismic bridge response," *Journal of Bridge Engineering*, vol. 8, no. 19, pp. 401–417, 2013.
[17] F. C. Ponzo, A. D. Cesare, G. Leccese, and D. Nigro, "Shaking table tests of a base isolated structure with double concave friction pendulum bearings," *Bulletin of the New Zealand Society for Earthquake Engineering*, vol. 48, no. 2, pp. 136–144, 2015.
[18] E. V. Monzon, I. G. Buckle, and A. M. Itani, "Seismic performance and response of seismically isolated curved steel I-girder bridge," *Journal of Structural Engineering*, vol. 142, no. 12, pp. 1–16, 2016.
[19] G. Abbiati, I. Lanese, E. Cazzador, O. S. Bursi, and A. Pavese, "Computational framework for fast-time hybrid simulation based on partitioned time integration and state-space modeling," *Structural Control and Health Monitoring*, vol. 26, no. 10, pp. 1–28, 2019.
[20] J. L. Almazan and J. C. De la Llera, "Analytical model of structures with frictional pendulum isolators," *Earthquake Engineering & Structural Dynamics*, vol. 31, no. 2, pp. 305–332, 2002.
[21] S. Barone, G. M. Calvi, and A. Pavese, "Experimental dynamic response of spherical friction-based isolation devices," *Journal of Earthquake Engineering*, vol. 23, no. 9, pp. 1465–1484, 2019.
[22] G. M. Calvi, P. Ceresa, C. Casarotti, D. Bolognini, and F. Auricchio, "Effects of axial force variation in the seismic response of bridges isolated with friction pendulum systems," *Journal of Earthquake Engineering*, vol. 8, no. sup001, pp. 187–224, 2004.
[23] P. Tsopelas, M. C. Constantinou, Y. S. Kim, and S. Okamoto, "Experimental study of FPS system in bridge seismic isolation," *Earthquake Engineering & Structural Dynamics*, vol. 25, no. 1, pp. 65–78, 1996.
[24] Z. Lai, X. Kang, L. Z. Jiang et al., "Earthquake influence on the rail irregularity on high-speed railway bridge," *Shock and Vibration*, vol. 2020, Article ID 4315304, 16 pages, 2020.
[25] JTG/T 2231-01-2020, *Specification for Seismic Design of Highway Bridges*, China: Ministry of Transport of the People's Republic of China, Beijing, China, 2020.
[26] GB 50011-2010, "Specification for seismic design of buildings," China: Ministry of Transport of the People's Republic of China, Beijing, China, 2010.
[27] W. X. Shi, K. Y. Liu, and L. Z. Wang, "Shaking table test study on damping performance of steel ball-bearing for grid structure," *Northwestern Seismological Journal*, vol. 31, no. 4, pp. 24–29, 2009.
[28] F. R. Xie, X. F. Cui, J. T. Zhao, Q. C. Chen, and H. Li, "Regionalization of the recent tectonic stress field in China and adjacent regions," *Chinese Journal of Geophysics*, vol. 47, no. 4, pp. 745–754, 2004.
[29] L. Yang, *Damage Characteristics of Large Span Continuous Beam Bridge under Multidimensional and Multiple Earthquake in High Speed Railway*, pp. 101–112, Central South University, Changsha, 2015.
[30] D. Yu, *Seismic Vulnerability Analysis for Prestressed Concrete Continuous Girder Bridge in High-Speed Railway*, pp. 99–121, Central South University, Changsha, 2015.
[31] G. Shao, L. Jiang, and N. Chouw, "Experimental investigations of the seismic performance of bridge piers with rounded rectangular cross-sections," *EARTHQUAKES AND STRUCTURES*, vol. 7, no. 4, pp. 463–484, 2014.